A Computational Study to Identify Potential Inhibitors of SARS-CoV-2 Main Protease (Mpro) from Eucalyptus Active Compounds

Ibrahim Ahmad Muhammad [1], Kanikar Muangchoo [2,*], Auwal Muhammad [3], Ya'u Sabo Ajingi [4], Ibrahim Yahaya Muhammad [3], Ibrahim Dauda Umar [3] and Abubakar Bakoji Muhammad [5,6]

[1] Department of Biochemistry, Faculty of Science, Kano University of Science and Technology (KUST), Wudil, Kano 713281, Nigeria; ibrahiem4real@gmail.com

[2] Faculty of Science and Technology, Rajamangala University of Technology Phranakhon (RMUTP), Bang Sue, Bangkok 10300, Thailand

[3] Department of Physics, Faculty of Science, Kano University of Science and Technology (KUST), Wudil, Kano 713281, Nigeria; auwal@kustwudil.edu.ng (A.M.); ibrahimyahayamuhammad@gmail.com (I.Y.M.); dauda6776@gmail.com (I.D.U.)

[4] Department of Biology, Faculty of Science, Kano University of Science and Technology (KUST), Wudil, Kano 713281, Nigeria; yausaboajingi@gmail.com

[5] Faculty of Natural Sciences II, Institute of Mathematics, Martin Luther University Halle-Wittenberg, 06099 Halle, Germany; abubakar.muhammad@mathematik.uni-halle.de

[6] Department of Mathematics, Faculty of Science, Gombe State University, Gombe 760214, Nigeria

* Correspondence: kanikar.m@rmutp.ac.th

check for updates

Abstract: Severe acute respiratory syndrome coronavirus 2 (SARS-CoV-2) was found to be a severe threat to global public health in late 2019. Nevertheless, no approved medicines have been found to inhibit the virus effectively. Anti-malarial and antiviral medicines have been reported to target the SARS-CoV-2 virus. This paper chose eight natural eucalyptus compounds to study their binding interactions with the SARS-CoV-2 main protease (Mpro) to assess their potential for becoming herbal drugs for the new SARS-CoV-2 infection virus. In-silico methods such as molecular docking, molecular dynamics (MD) simulations, and Molecular Mechanics Poisson Boltzmann Surface Area (MM/PBSA) analysis were used to examine interactions at the atomistic level. The results of molecular docking indicate that Mpro has good binding energy for all compounds studied. Three docked compounds, α-gurjunene, aromadendrene, and allo-aromadendrene, with highest binding energies of -7.34 kcal/mol (-30.75 kJ/mol), -7.23 kcal/mol (-30.25 kJ/mol), and -7.17 kcal/mol (-29.99 kJ/mol) respectively, were simulated with GROningen MAchine for Chemical Simulations (GROMACS) to measure the molecular interactions between Mpro and inhibitors in detail. Our MD simulation results show that α-gurjunene has the strongest binding energy of -20.37 kcal/mol (-85.21 kJ/mol), followed by aromadendrene with -18.99 kcal/mol (-79.45 kJ/mol), and finally allo-aromadendrene with -17.91 kcal/mol (-74.95 kJ/mol). The findings indicate that eucalyptus may be used to inhibit the Mpro enzyme as a drug candidate. This is the first computational analysis that gives an insight into the potential role of structural flexibility during interactions with eucalyptus compounds. It also sheds light on the structural design of new herbal medicinal products against Mpro.

Keywords: binding energy; eucalyptus compounds; molecular docking; molecular dynamics; SARS-CoV-2

1. Introduction

Unspecified pneumonia was reported in the Wuhan region of the Hubei Province, China, towards the end of 2019. Medically, it was quite comparable to viral pneumonia. After the screening of clinical samples, the disease control unit specialist reported that it was pneumonia associated with the severe acute respiratory syndrome (SARS). Eventually, the World Health Organization (WHO) officially labeled it COVID-19 and it has quickly spread from its original area to nearly all of China, and over 200 nations and regions worldwide today. The International Committee on Virus Taxonomy called the new coronavirus "severe acute respiratory syndrome coronavirus 2" (SARS-CoV-2) [1,2]. The SARS-CoV-2 infection leads to difficulty breathing, fever, chronic respiratory failure, and dry cough, which might also result in death [3]. A total of 14,263,202 SARS-CoV-2 cases were recorded as of 20 July 2020, with 220,026 new confirmed cases and 602,244 deaths worldwide [4]. Nigeria alone recorded 36,663 confirmed cases and 789 fatalities. Cases increased exponentially between April and June, with the highest number of cases reported on 15 June (904 confirmed cases) and 45 deaths reported on 18 June 2020 [5].

SARS-CoV-2 is part of the Coronaviridae family that consists of the main positive-sense single-strand RNA viruses. These viruses are categorized into α, β, γ, and δ genera. SARS-CoV-2, SARS-CoV, and Middle East respiratory syndrome coronavirus (MERS-CoV) all belong to β-coronaviruses. A study of the genome sequences of these viruses showed that SARS-CoV-2 encompasses a higher nucleotide homology of 89.1% with SARS-CoV compared with MERS-CoV [1,3,6]. In spite of the scientific community's immediate and unprecedented research efforts worldwide, no successful antiviral or vaccine is currently available for SARS-CoV-2. Nevertheless, substantial steps have been taken to produce vaccines and treatment drugs undergoing early clinical studies. Antiviral medicines such as remdesivir developed for Ebola, and anti-HIV drugs such as lopinavir and ritonavir, and popular anti-malaria medicine hydroxychloroquine are currently in mega clinical testing for COVID-19 treatments [7]. Some studies have revealed that chloroquine phosphate inactivates SARS-CoV-2 [8–10], and others revealed that SARS-CoV-2 in-vitro is inhibited by hydroxychloroquine sulfate [8,10]. In addition, computational scientists used the in-silico strategy to identify potential drug targets by investigating complex atomistic interactions [11–15]. One of the most described drug targets for SARS-CoV-2 is the main protease (Mpro, also called 3CLpro), an enzyme necessary for the viral replication. The Mpro works in at least 11 digestive sites in the gigantic polypeptide 1ab (replicase 1ab, approximately 790 kDa) [16].

Based on recent economic impacts on the financial markets, vaccine manufacturing funding appears to be a considerable investment in the coming days [17]. Natural drug treatment may help to avert the spread of the virus in this setting. Nature offers a vast library of chemical compounds that have yet to be researched and established as medicines for the therapy of many viral infections [18]. The eucalyptus tree is one of several plant species used in Nigeria to prevent certain diseases. Customarily, the leaves are boiled, and the fumes are breathed to increase the respiratory tract's effectiveness. East Africa's Mozambique report suggested that eucalyptus could assist in combating malaria, flu, and even fever, reducing the transmission of the disease outbreak. However, national health specialists in the country are often warning of eucalyptus vapor inhalation [19]. Since prehistoric times eucalyptus has been used for many reasons because it has anti-cancer, anti-inflammatory, antiseptic, antioxidant, and antibacterial properties. Therefore, common colds, flu, sinus congestion, and respiratory ailments are cured with eucalyptus [20]. Bahare Salehi et al. (2019) also reported that eucalyptus had gained a great deal of global interest due to its antimicrobial, anti-inflammatory, and insect repellent properties for therapeutic and furniture purposes. The most significant medical benefits of eucalyptus include improving respiratory health, boosting the immune system, lowering blood pressure, and combating bacterial infection. Traditionally, it is being used to promote mucus secretion in the respiratory system [21].

The head of the Indonesian Ministry of Agriculture has recently admitted that eucalyptus-dependent treatment has been established, stating that the spread of COVID-19 has therefore been decreased. Influenza, β, and γ coronaviruses were screened, and 80–100% of the viruses

had been destroyed [22]. However, in less than a month, another analysis revealed that the efficacy of eucalyptus oil in COVID-19 therapy still requires extra study, since COVID-19 (SARS-CoV-2) was not included in earlier studies, but other forms of coronavirus were. Hence, as a result of this limited research data, eucalyptus cannot merely be referred to as the SARS-CoV-2 drug [23]. For this research work, eight eucalyptus compounds were selected for use against the target SARS-CoV-2 Mpro. As an in-silico technique, molecular docking simulation was used to understand the positional binding and interaction mechanisms with the target molecule. To further investigate the nature of the interactions and the energy contribution per amino acid residue, the top three compounds with the best (lowest in terms of kcal/mol) binding energies were subjected to classical molecular dynamics simulations. To the best of our knowledge, this is the first computational report that explores the potential inhibitory effects of eucalyptus compounds against the Mpro protein.

2. Methods

2.1. Ligand Preparations

The information about eight compounds selected from eucalyptus with antiviral activities was reported from the literature [20,21,24,25]. Such compounds were found in the PubChem database [26] and saved in .sdf format, then translated into three-dimensional structures with Avogadro software [27]. ChemSketch was used to create two-dimensional structures of the phytochemicals (Figure 1). PubChem ID and the molecular weight are listed in Table 1.
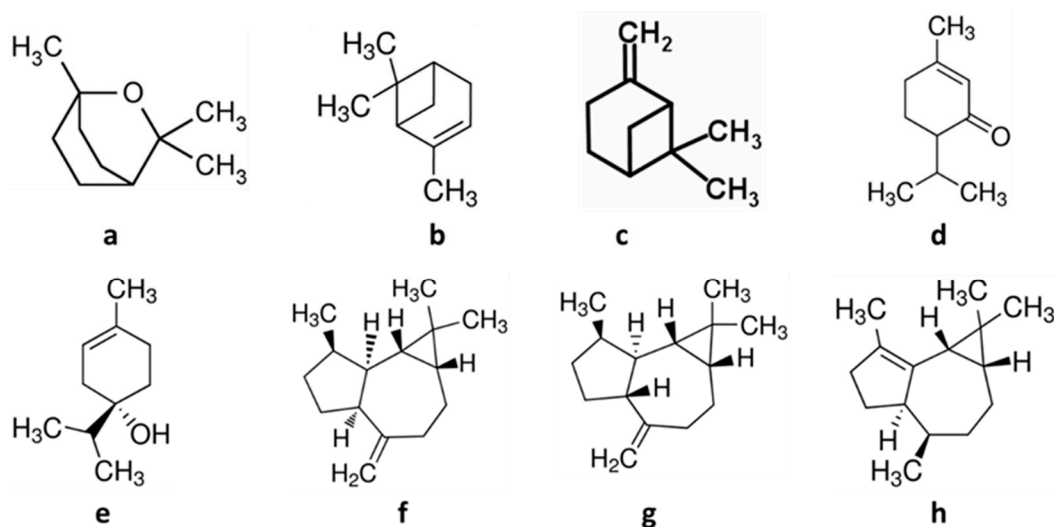

Figure 1. Two molecular dimensional structures of the eucalyptus compounds used in this study: (**a**) 1, 8-cineole (eucalyptus), (**b**) α-pinene, (**c**) β-pinene, (**d**) terpinen-4-ol, (**e**) piperitone, (**f**) allo-aromadendrene, (**g**) aromadendrene, and (**h**) α-gurjunene.

Table 1. PubChem ID and molecular weight of the selected compounds.

Eucalyptol Compounds	PubChem ID	Molecular Weight (g/mol)
1,8-cineole (eucalyptol)	2758	154.25
α-pinene	440968	136.23
β-pinene	440967	136.23
Terpinen-4-ol	11230	154.25
Piperitone	92998	168.23
Allo-aromadendrene	42608158	204.35
Aromadendrene	91354	204.35
α-gurjunene	15560276	204.35

2.2. Protein Model Preparations

The SARS-CoV-2 Mpro 3D structure (Figure 2) with PDB ID: 6LU7 [28] was from the protein database library (https://www.rcsb.org). The structure was imported into visual molecular software, eliminating a ligand (N3) in complex with protein and water molecules. Hydrogen atoms were added prior to docking to correct the ionization and tautomeric states of amino acid residues. There are three different domains in the Mpro structure: residues from domain I (8–100), residues from domain II (101–183), and residues from domain III (200–303). N-terminal amino acids 1 through 7 constitute the N-finger, which plays an essential role in dimerizing and forming the Mpro active site. Domains I and II, known collectively as the N-terminal domain, have an anti-parallel β-sheet structure with 14 β-strands. The substrate-binding site is positioned inside a cleft between domains I and II. A loop from amino acids 184 to 199 connects the N-terminal domain and domain III, also known as the C-terminal domain, and forms a five α-helix anti-parallel cluster [29].
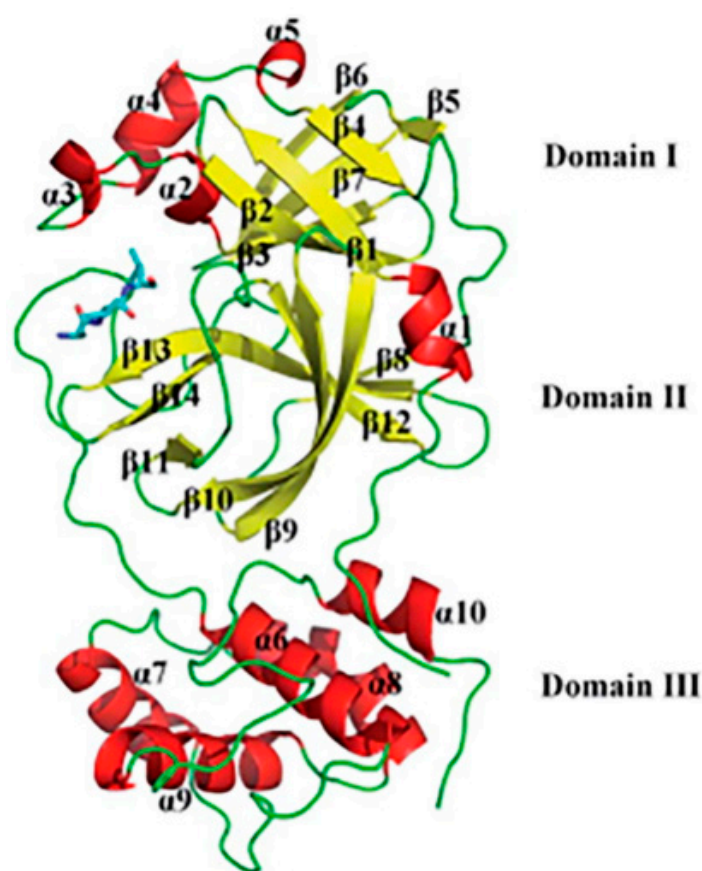

Figure 2. Three-dimensional structure of Mpro protein in complex with N3 inhibitor. It comprises three different domains.

2.3. Molecular Docking

Molecular docking was performed using Autodock4.2 [30] to test the binding affinity of eucalyptus compounds toward the SARS-CoV-2 Mpro protein molecule. The receptor molecule remained rigid, and ligands were versatile to achieve a degree of freedom associated with rotational parameters. Protein and ligand PDB were transformed into .pdbqt after merging the nonpolar hydrogen. The cubical grid box had a size of $126 \times 126 \times 126$ and a spacing of 0.375 Å. A rigid grid box was used for the Autogrid4 parameter. In addition to Autogrid, Autodock4 with Lamarckian genetic algorithms [31] was used to achieve optimal docking conformations. Default docking parameters were used except for the docking run. There was a total of one hundred docking runs per compound. The binding affinity more clearly

explains the inhibitor's interaction with the protein molecule. The compound's most desirable binding poses were examined by choosing the lowest free energy of binding (ΔG) and the lowest inhibition constant (Ki). The inhibition constant was calculated theoretically with the help of Autodock4.2. Between a protein and ligand, a stable complex was formed, exhibiting more negative free energy from binding and low Ki indicating high potency of an inhibitor [32]. For further analysis, three compounds with the lowest binding energies were selected for the starting structure to set up molecular dynamics simulations. The interactions between the compounds and the target enzyme were studied using Ligplot+ [33].

2.4. Molecular Dynamics (MD) Simulations and Analysis

The GROMACS 2019.3 package was used to perform MD simulations using selected complexes with the lowest binding energies. The complexes were solvated with TIP3P water molecules, which were constrained by LINCS [34] and SETTLE [35] algorithms. Four Na+ counter-ions were added to neutralize the simulation system's charge, and energy minimization was performed using the steepest descent algorithm and GROMOS54A7 force field [36] with a corresponding equilibration of 1 ns. MD simulation was performed for 100 ns per system. Our previous MD studies described a thorough procedure [37]. Molecular mechanics of Poisson–Boltzmann surface area (MM-PBSA) techniques were used to calculate the free binding energies of the complexes. MM-PBSA enthalpy was calculated using molecular mechanics. The effects of both polar and nonpolar solvent components on free energy were evaluated using the Poisson–Boltzmann equation. For the calculation of energy, the GROMACS built-in tools g_mmpbsa and APBSA [38] were used. The last 30 ns of MD simulations were taken in each complex with 3000 frames in each. The parameters used in g_mmpbsa calculations included a protein dielectric constant of 4, solvent dielectric constant set to 80, vacuum dielectric constant set to 1, temperature of 303 K, and SASA constant and surface tension set to 3.84982 kJ/mol and 0.0226778 kJ/(mol Å^2) respectively.

3. Results

3.1. Molecular Docking Results

The molecular docking technique has become one of the most used methods for determining the drug targets for ligand-based computer-aided drug discovery (LB-CADD). This approach has now been used to analyze vast data from drug repositories and easily register, which can save enormous resources, time, and expense associated with LB-CADD [39]. Until now, successful drug treatment for the SARS-CoV-2 virus has not been approved, and it is urgently necessary to identify possible drug targets. We used in-silico Autodock4 to identify possible binding sites and interaction mechanisms of eight potential natural eucalyptus compounds against the Mpro protein of SARS-CoV-2. The tested compounds will pave the way for the development of drugs against SARS-CoV-2. After the docking simulation, 100 different poses of small molecules (ligands) were produced among which the pose with the strongest binding affinity was considered the best pose.

The findings obtained after the docking analysis are described in Table 2 regarding ligand binding energy (kcal/mol), inhibition constant (K$_i$), and Mpro amino acid residues interacting with natural compounds. The active site of Mpro protein was found to bind all compounds with a range of amino acid residues engaged in interactions. These interactions have been linked to proof of the in-silico protein-ligand interactions. Figure 3 demonstrates the docked natural compound molecules in complexes with Mpro protein. Three of the natural compounds, α-gurjunene, aromadendrene, and allo-aromadendrene, showed significant binding with binding energies of −7.34 kcal/mol (−30.71 kJ/mol), −7.23 kcal/mol (−30.25 kJ/mol), and −7.17 kcal/mol (−29.99 kJ/mol), respectively.

Table 2. Estimated lowest binding energies of main protease (Mpro) in complex with eucalyptus compounds obtained from molecular docking calculations along with inhibition constants and interaction residues.

Eucalyptol Compounds	Binding Energy (kJ/mol)	Inhibition Constant (Ki) (μM)	Mpro Residues Interacting with Natural Compounds
1,8-cineole (eucalyptol)	−26.90	19.5	His41, Met49, Tyr54, His164, Met165, Asp187, Arg188, and Gln189
α-pinene	−26.23	25.55	His41, Met49, His164, Met165, Asp187, Arg188, and Gln189
β-pinene	−26.57	22.34	His41, Met49, Tyr54, His164, Met165, Asp187, Arg188, and Gln189
Terpinen-4-ol	−23.89	65.5	His41, Met49, Pro52, Tyr54, His164, Arg188, and Gln189
Piperitone	−25.52	33.95	His41, Met49, Tyr54, Cys145, His164, Met165, Glu166, Asp187, and Arg188
Allo-aromadendrene	−29.99	5.54	His41, Met49, Tyr54, Cys145, His164, Met165, Glu166, Asp187, Arg188, and Gln189
Aromadendrene	−30.25	5.06	His41, Met49, Tyr54, Cys145, His164, Met165, Asp187, Arg188, and Gln189
α-gurjunene	−30.71	4.15	His41, Met49, Tyr54, Cys145, His164, Met165, Glu166, Asp187, Arg188, and Gln189

The residue of amino acids that led to the binding of Mpro and natural molecules was achieved through hydrophobic and hydrogen bond interactions. Molecular interactions generally play a significant role in forming and stabilizing docking complexes [40,41]. Hydrophobic interactions with eight amino acid residues (His41, Met49, Tyr54, His164, Met165, Asp187, Arg188, and Gln189) have been observed involving eucalyptus with the binding energy of −6.43 kcal/mol (−26.90 kJ/mol) (Figure 4a). The α-pinene compound made a complex through AutoDock with the binding energy of −6.27 kcal/mol (−26.23 kJ/mol). The hydrophobic interactions were formed by seven amino acid residues His41, Met49, His164, Met165, Asp187, Arg188, and Gln189 (Figure 4b). Nearly the same activity with the β-Pinene compound was observed in contrast to α-pinene with the addition of one amino acid residue, Tyr54 (Figure 4c). The binding energy of the terpinen-4-ol molecule was −5.71 kcal/mol (−23.89 kJ/mol), His164 residue formed a hydrogen bond, and six residues of His41, Met49, Pro52, Tyr54, Arg188, and Gln189 were associated in hydrophobic interactions (Figure 4d). Even though the terpinen-4-ol compound had less binding energy in all, it was found relatively useful to bind with active residues. The docked binding energy of the piperitone substrate was −6.1 kcal/mol (−25.52 kJ/mol). At the active site of Mpro, there was one hydrogen bond formation with His164, while eight amino acids were engaged in the formation of hydrophobic interactions (Figure 4e). The binding energy of allo-aromadendrene was −7.17 kcal/mol (−29.99 kJ/mol) and it interacted with nine amino acid residues (His41, Met49, Tyr54, Cys145, His164, Met165, Glu166, Asp187, Arg188, and Gln189) in the active site of SARS-CoV-2 Mpro. These residues participated in hydrophobic interactions (Figure 4f). The compounds aromadendrene and α-gurjunene with binding energies of −7.23 kcal/mol (−30.25 kJ/mol) and −7.34 kcal/mol (−30.71 kJ/mol) formed van der Waals interactions with seven specific amino acid residues (His41, Met49, Cys145, Met165, Asp187, Arg188, and Gln189). Such molecules had the strongest binding energies in contrast with six other molecules (Figure 4g,h). Earlier studies support our findings by reporting similar amino acid residues to SARS-CoV-2 Mpro protein interactions with other ligands, as confirmed in our study [16,29,42–44].
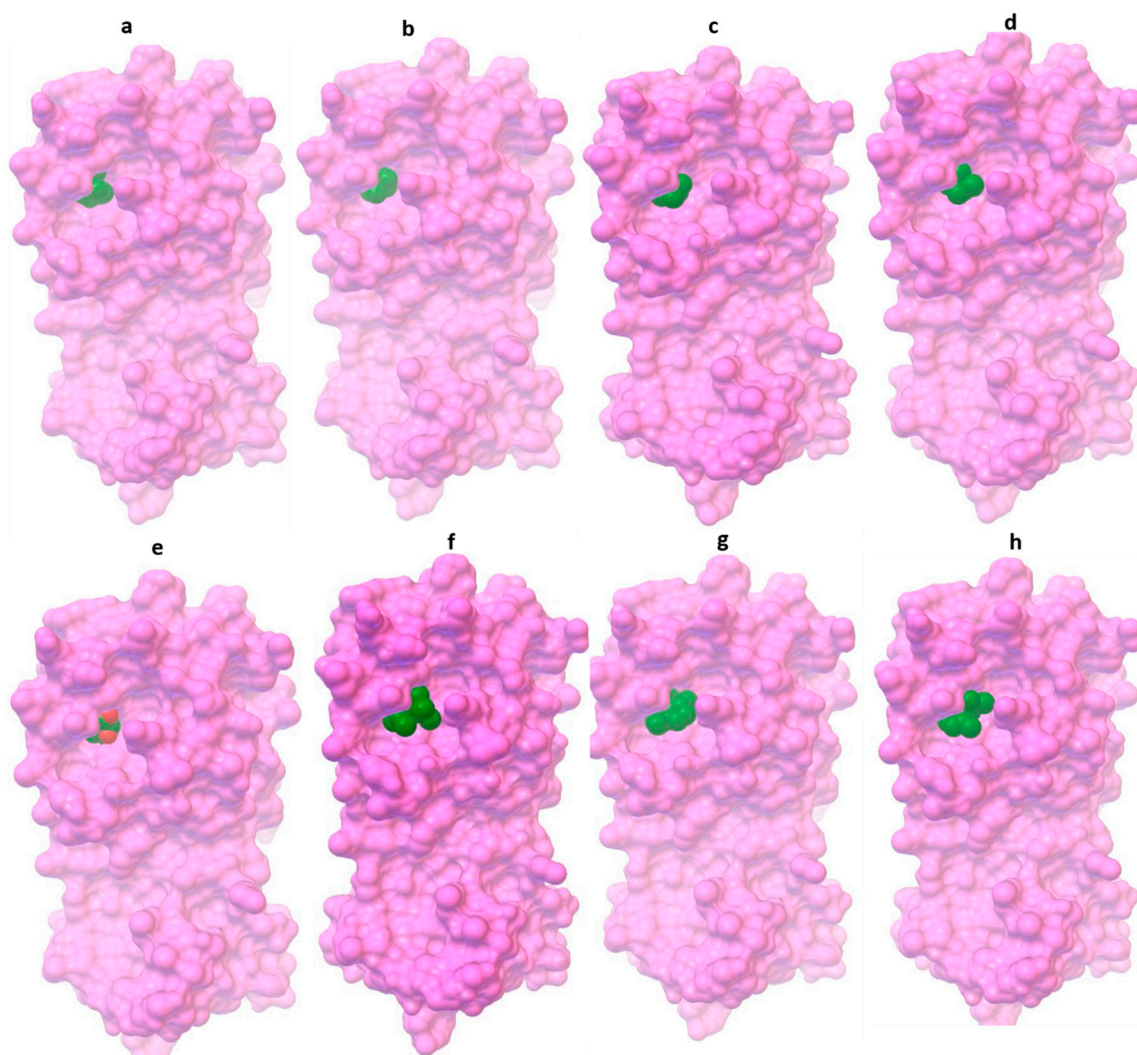
Figure 3. Docking structure of Mpro in complex with eucalyptus compounds: (**a**) 1, 8-cineole (eucalyptus), (**b**) α-pinene, (**c**) β-pinene, (**d**) terpinen-4-ol, (**e**) piperitone, (**f**) allo-aromadendrene, (**g**) aromadendrene, and (**h**) α-gurjunene.

3.2. MD Simulations

Classical MD simulations are one of the computer simulation techniques for atomic resolution dynamic molecular data [45]. The three natural compounds (α-gurjunene, aromadendrene, and allo-aromadendrene) in complex with Mpro protein underwent MD simulations of 100 ns to evaluate the interactions in more detail and the per residue energy contributions of each amino acid. To evaluate the stability of the selected structures, the root mean square deviation (RMSD) of protein and ligand was calculated for 100 ns trajectories. In addition, the root mean square fluctuation (RMSF) values for each residue were analyzed to assess the local flexibility.

Changes were observed, as expected, for both protein conformations and positional ligand binding. Conformational changes as a function of time were monitored by RMSD measurements, in which α-gurjunene induced major conformational changes. Different trends have been identified in the measurement of RMSF, which indicate that domain I, part of domain II, and domain III regions were significantly influenced by protein conformation variations. Aromadendrene and allo-aromadendrene RMSD values were lower than α-gurjunene, suggesting that these ligands may stabilize protein conformations. Further, in the early stages of MD (around 10 ns), the behavior of α-gurjunene shifted and increased suddenly from 0.2 nm to almost 0.8 nm. In about 60 ns, the structure stabilized and had higher RMSD values than aromadendrene

and allo-aromadendrene (Figure 5a). The overall average RMSF values were shown to be unstable at residues (8–100), (163–200), and (200–305), respectively (Figure 5b). For α-gurjunene, a lower RMSF value was noticed, followed by aromadendrene and allo-aromadendrene. Lower RMSF values suggest more excellent stability and the natural compound's possibility to inhibit the target molecule [37,46]. Changes in ligand positioning have also been monitored by the ligand RMSD measurement, as shown in Figure 5c. The α-gurjunene molecule (red) was transferred to domain II of the Mpro protein in the earliest stage of MD simulation and lasted for 15.6 ns. The RMSD of the ligand reached its peak at around 4.8 nm, falling immediately to 3.5 nm and stabilized over the remaining time (ns) and bound to domain III for the last 84 ns. The behavior of the α-gurjunene might be due to its unique structure compared to the other two ligands. This structural peculiarity may account for the instability of the ligand at the earlier stage of the simulation. Although in the case of aromadendrene and allo-aromadendrene ligands, they remained intact during the simulation time with the Mpro molecule.
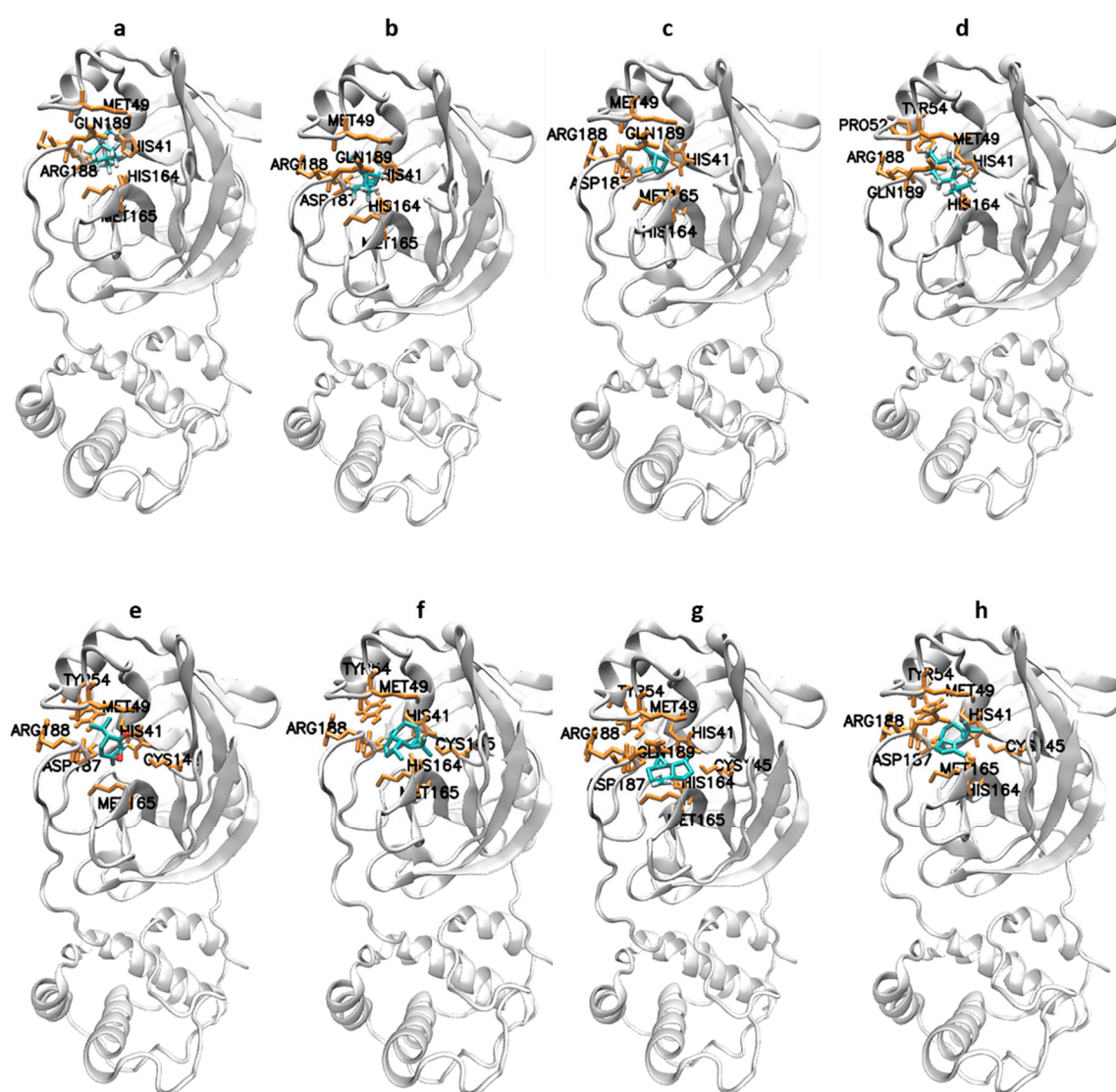

Figure 4. Predicted binding amino acid residues from the docking simulation of Mpro in complex with (**a**) 1, 8-cineole (eucalyptus), (**b**) α-pinene, (**c**) β-pinene, (**d**) terpinen-4-ol, (**e**) piperitone, (**f**) allo-aromadendrene, (**g**) aromadendrene, and (**h**) α-gurjunene.
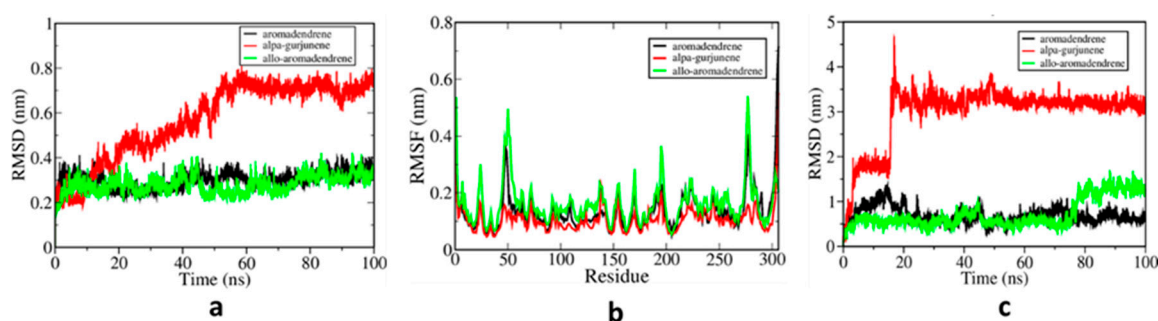
Figure 5. (**a**) Root mean square deviation (RMSD) of backbone carbon (Cα) atomic positions of the Mpro relative to the starting structure measured from the 100 ns trajectories, (**b**) per residue root mean square fluctuations (RMSF) of Cα atomic positions measured over the last 30 ns from protein conformations, and (**c**) RMSD of ligand atomic positions relating to the starting structure measured from the 100 ns trajectories with allo-aromadendrene (green), aromadendrene (black), and α-gurjunene (red).

MM/PBSA calculations were carried out on the last 30 ns of all simulations to examine further inhibitory effects and the interaction networks between Mpro protein and natural molecules (ligands). Table 3 presents a description of the MM/PBSA energy, van der Waals, electrostatic, polar, and apolar solvation energy contributions. Figure 6 shows per residue energy contribution within the binding site given by MM/PBSA energy decomposition. In all, the contributions of van der Waals were stronger, suggesting substantially higher hydrophobic energy contributions with energies of −23.66 ± 2.04 kcal/mol (−99.00 ± 8.53 kJ/mol), −21.23 ± 2.89 kcal/mol (−88.82 ± 12.08 kJ/mol), and −21.66 ± 2.33 kcal/mol (−90.61 ± 9.73 kJ/mol) respectively for α-gurjunene, aromadendrene, and allo-aromadendrene. The strongest total binding energy of −20.37 ± 2.26 kcal/mol (−85.21 ± 9.44 kJ/mol) was found in α-gurjunene, which was higher in van der Waals energy than in aromadendrene and allo-aromadendrene with binding energies of −18.99 ± 3.02 kcal/mol (−79.45 ± 12.62 kJ/mol) and −17.91 ± 2.12 kcal/mol (−74.95 ± 8.88 kJ/mol) respectively. The results for total binding energy were lower than the experimental binding energies of protein in complex with small organic molecules, as reported by [47]. The authors determined the experimental binding energy values ranging from −20.80 kcal/mol (−87.03 kJ/mol) to −37.80 kcal/mol (−158.16 kJ/mol).

Table 3. Binding energy obtained using MM/PBSA technique of each complex along with contributions from van der Waals, electrostatic, polar and apolar solvation energies.

Complex Structures	Van der Waals Energy (±SD) (kJ/mol)	Electrostatic Energy (±SD) (kJ/mol)	Polar Solvation Energy (±SD) (kJ/mol)	Apolar Energy (±SD) (kJ/mol)	Total Binding Energy (±SD) (kJ/mol)
Mpro-allo-aromadendrene	−90.61 (±9.73)	−2.06 (±6.57)	27.31 (±5.34)	−9.59 (±1.23)	−74.95 (±8.88)
Mpro-aromadendrene	−88.82 (±12.08)	−3.42 (±4.77)	21.89 (±4.92)	−9.11 (±1.25)	−79.45 (±12.62)
Mpro-α-gurjunene	−99.00 (±8.53)	−0.33 (±1.91)	25.55 (±6.93)	−11.42 (±1.06)	−85.21 (±9.44)

We also validated the binding energies of the compounds tested in our study with some selected co-crystallized ligands, as presented in Table 4. Compared to the estimated binding energy of co-crystallized ligands, darunavir has a better estimated binding energy value. Based on this finding, ΔG of darunavir was used as a standard in calculating the change in binding energy (ΔΔG) of other ligands. The result showed that the selected eucalyptus compounds could be favorable inhibitors of the Mpro enzyme. This suggests that these small molecules could serve as potential drug candidates for SARS-CoV-2 treatment.
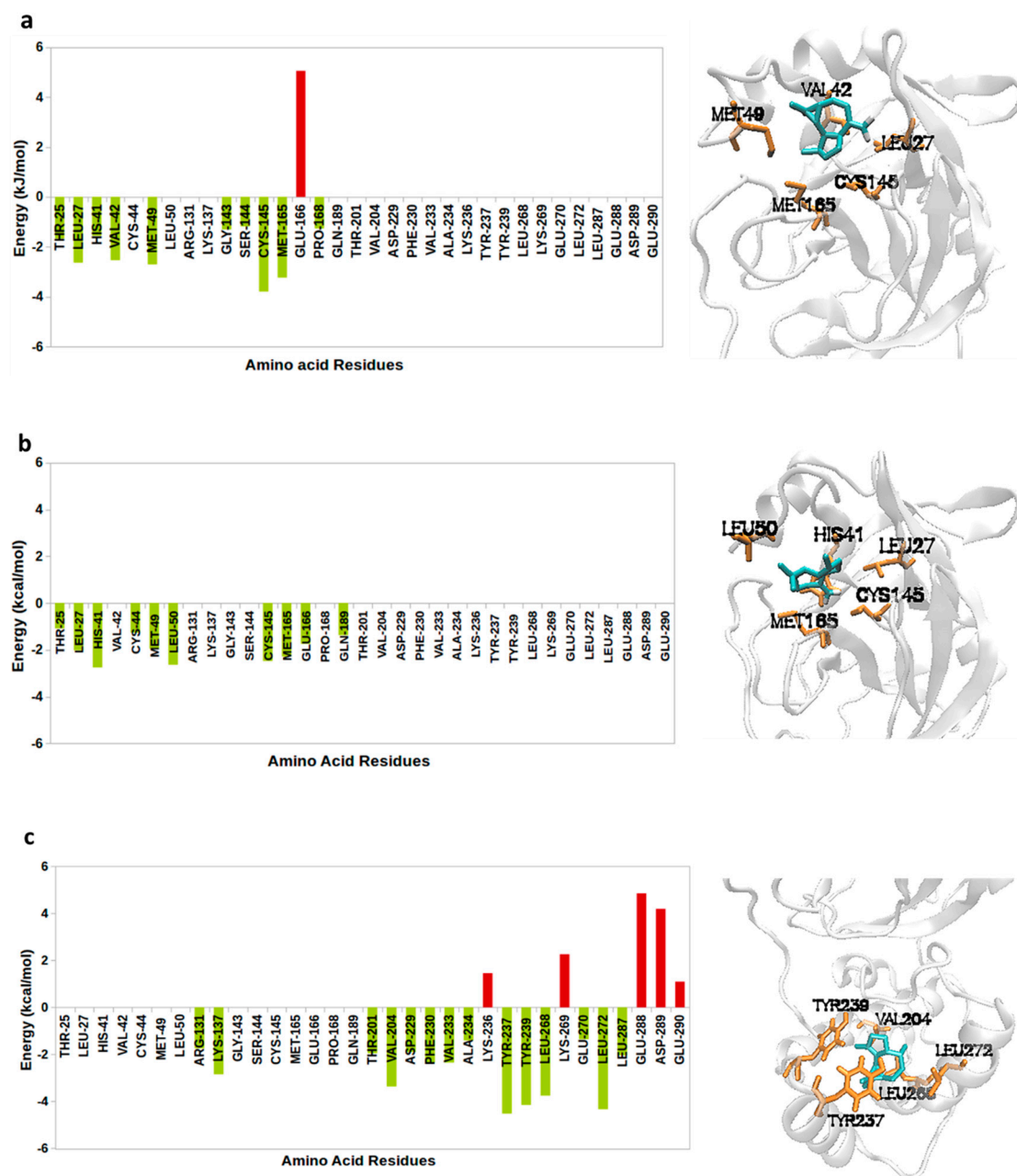
Figure 6. Per residue energy contributions (in kJ/mol) of the inhibitors. Red bars represent amino acids with unfavorable binding energies while light green bars represent amino acids with favorable binding energies; (right) final molecular dynamics (MD) snapshots of the major residues that contributed to the binding of Mpro in complex with (**a**) allo-aromadendrene, (**b**) aromadendrene, and (**c**) α-gurjunene.

Table 4. Estimated binding energies of co-crystalized ligands against selected eucalyptus compounds.

Ligands	Estimated Binding Energy (kJ/mol)	Estimated ΔΔG (kJ/mol)	Reference
N3	−51.07	−44.46	[48]
Indinavir	−72.11	−23.42	[48]
Darunavir	−95.53	-	[48]
Favipiravir	−36.07	−59.46	[49]
Fosfomycin	−60.63	−34.90	[49]
Aspirin	−78.37	−17.16	[49]
Allo-aromadendrene	−74.95	−20.58	This study
Aromadendrene	−79.45	−16.08	This study
α-gurjunene	−85.21	−10.32	This study

In addition, MM/PBSA energy decomposition was used to obtain the individual contributions of amino acids to the binding energy, revealing significant active site interaction residues. Mpro-allo-aromadendrene bound Thr25, Leu27, His41, Met49, Gly143, Ser144, Cys145, Met165, and Pro168 (Figure 5a). Residues such as Glu166 showed higher positive values, implying unfavorable interactions due to the steric obstruction effect caused by repulsive forces. In aromadendrene, the primary amino acid contributors were Thr25, Leu27, His41, Cys44, Met49, Leu50, Cys145, Met165, Glu166, and Gln189 respectively (Figure 5b). The energy per residue was comparable to previous analyses of MD simulations with several SARS-CoV-2 Mpro inhibitors and according to our findings [50–52].

Mpro-α-gurjunene found Lys237, Val204, Phe230, Val233, Tyr237, Tyr239, Leu268, and Leu272 as the most desirable residues (Figure 5c). Further, the residues dominated by the amino acids with hydrophobic and polar uncharged side chains were actively involved. Thus, the strongest values of van der Waals interaction and the nonpolar component of the solvation energy component correspond to the favorable strength of α-gurjunene. Nevertheless, Lys236, Lys269, Glu288, Asp289, and Glu290 displayed unfavorable (positive) interactions, which may be attributable to steric impact and binding opposition. The amino acid residues found in MD simulations were not identical to docking. The principal explanation for this may be the shift of the α-gurjunene in the simulations. This investigation is the first to elucidate the detailed atomistic interactions of eucalyptus phytochemical compounds with the SARS-CoV-2 main protease. For the first time, some new participating amino acids have been reported in another binding site surplus to the active site residues found in Mpro. Eucalyptus has been a traditional medicinal plant for decades, and as a result of this study it could be used as a potential therapeutic drug candidate to suppress the replicative function of the main protease.

4. Conclusions

Due to severe outbreaks and lack of effective drugs, the new coronavirus has become a global concern. Therefore, recovery strategies need to be identified and tested more efficiently. In this regard, in-silico processes are very efficient and helpful. Throughout this research, various computational techniques such as molecular docking, MD simulations, and MM-PBSA calculations have been used to classify novel natural compounds as potential inhibitors for Mpro, the SARS-CoV-2 protein. Eight eucalyptus phytochemical compounds were used here for screening purposes. Based on molecular docking assessments, all eight compounds bound to the binding pocket with strong binding affinities. For further analysis, three molecules (α-gurjunene, aromadendrene, and allo-aromadendrene) with the lowest inhibition constant values were chosen. Eventually, from MD simulation results, we found that all molecules could bind to the target protein with the strongest binding affinities. Such findings have indicated that these compounds could be considered as novel natural molecules for the possible development of appropriate SARS-CoV-2 drug candidates. These results are in line with the recent research that shows that eucalyptus is successful in treating the new coronavirus.

Author Contributions: Conceptualization, K.M.; methodology, A.M.; software, A.M.; validation, I.A.M. and Y.S.A.; formal analysis, A.B.M.; investigation, Y.S.A. and I.Y.M.; resources, K.M.; writing—original draft preparation, I.A.M.; writing—review and editing, A.M. and Y.S.A.; visualization, I.Y.M. and I.D.U.; supervision, K.M.; project administration, K.M.; funding acquisition, K.M. All authors have read and agreed to the published version of the manuscript.

Conflicts of Interest: The authors declare no conflict of interest.

References

1. Macchiagodena, M.; Pagliai, M.; Procacci, P. Identification of potential binders of the main protease 3CLpro of the COVID-19 via structure-based ligand design and molecular modeling. *Chem. Phys. Lett.* **2020**, *750*, 137489. [CrossRef] [PubMed]

2. Wang, L.; Wang, Y.; Ye, D.; Liu, Q. Review of the 2019 novel coronavirus (SARS-CoV-2) based on current evidence. *Int. J. Antimicrob. Agents* **2020**, *55*, 105948. [CrossRef] [PubMed]

3. Jin, Y.-H.; Cai, L.; Cheng, Z.-S.; Cheng, H.; Deng, T.; Fan, Y.-P.; Fang, C.; Huang, D.; Huang, L.-Q.; Huang, Q.; et al. A rapid advice guideline for the diagnosis and treatment of 2019 novel coronavirus (2019-nCoV) infected pneumonia (standard version). *Mil. Med. Res.* **2020**, *7*, 4. [CrossRef] [PubMed]

4. WHO. WHO Coronavirus Disease (COVID-19) Dashboard. Available online: https://covid19.who.int/ (accessed on 20 July 2020).

5. WHO. Global Nigeria WHO (COVID-19) Homepage. Available online: https://covid19.who.int/region/afro/country/ng (accessed on 20 July 2020).

6. He, J.; Hu, L.; Huang, X.; Wang, C.; Zhang, Z.; Wang, Y.; Zhang, D.; Ye, W. Potential of coronavirus 3C-like protease inhibitors for the development of new anti-SARS-CoV-2 drugs: Insights from structures of protease and inhibitors. *Int. J. Antimicrob. Agents* **2020**, *56*, 106055. [CrossRef]

7. Delang, L.; Neyts, J. Medical treatment options for COVID-19. *Eur. Heart J. Acute Cardiovasc. Care* **2020**, *9*, 209–214. [CrossRef]

8. Liu, J.; Cao, R.; Xu, M.; Wang, X.; Zhang, H.; Hu, H.; Li, Y.; Hu, Z.; Zhong, W.; Wang, M. Hydroxychloroquine, a less toxic derivative of chloroquine, is effective in inhibiting SARS-CoV-2 infection in vitro. *Cell Discov.* **2020**, *6*, 16. [CrossRef]

9. Wang, M.; Cao, R.; Zhang, L.; Yang, X.; Liu, J.; Xu, M.; Shi, Z.; Hu, Z.; Zhong, W.; Xiao, G. Remdesivir and chloroquine effectively inhibit the recently emerged novel coronavirus (2019-nCoV) in vitro. *Cell Res.* **2020**, *30*, 269–271. [CrossRef]

10. Yao, X.; Ye, F.; Zhang, M.; Cui, C.; Huang, B.; Niu, P.; Liu, X.; Zhao, L.; Dong, E.; Song, C.; et al. In Vitro Antiviral Activity and Projection of Optimized Dosing Design of Hydroxychloroquine for the Treatment of Severe Acute Respiratory Syndrome Coronavirus 2 (SARS-CoV-2). *Clin. Infect. Dis.* **2020**, *71*, 732–739. [CrossRef]

11. Eleftheriou, P.; Amanatidou, D.; Petrou, A.; Geronikaki, A. In Silico Evaluation of the Effectivity of Approved Protease Inhibitors against the Main Protease of the Novel SARS-CoV-2 Virus. *Molecules* **2020**, *25*, 2529. [CrossRef]

12. Hall, D.C., Jr.; Ji, H.-F. A search for medications to treat COVID-19 via in silico molecular docking models of the SARS-CoV-2 spike glycoprotein and 3CL protease. *Travel. Med. Infect. Dis.* **2020**, *35*, 101646. [CrossRef]

13. Kumar, Y.; Singh, H.; Patel, C.N. In silico prediction of potential inhibitors for the Main protease of SARS-CoV-2 using molecular docking and dynamics simulation based drug-repurposing. *J. Infect. Public Health* **2020**, *13*, 1210–1223. [CrossRef] [PubMed]

14. Prasanth, D.S.N.B.K.; Murahari, M.; Chandramohan, V.; Panda, S.P.; Atmakuri, L.R.; Guntupalli, C. In silico identification of potential inhibitors from Cinnamon against main protease and spike glycoprotein of SARS CoV-2. *J. Biomol. Struct. Dyn.* **2020**, 1–15. [CrossRef]

15. Yu, R.; Chen, L.; Lan, R.; Shen, R.; Li, P. Computational screening of antagonists against the SARS-CoV-2 (COVID-19) coronavirus by molecular docking. *Int. J. Antimicrob. Agents* **2020**, *56*, 106012. [CrossRef] [PubMed]

16. Zhang, L.; Lin, D.; Sun, X.; Curth, U.; Drosten, C.; Sauerhering, L.; Becker, S.; Rox, K.; Hilgenfeld, R. Crystal structure of SARS-CoV-2 main protease provides a basis for design of improved α-ketoamide inhibitors. *Science* **2020**, *368*, 409–412. [CrossRef] [PubMed]

17. Amanat, F.; Krammer, F. SARS-CoV-2 Vaccines: Status Report. *Immunity* **2020**, *52*, 583–589. [CrossRef] [PubMed]

18. Denaro, M.; Smeriglio, A.; Barreca, D.; De Francesco, C.; Occhiuto, C.; Milano, G.; Trombetta, D. Antiviral activity of plants and their isolated bioactive compounds: An update. *Phytother. Res.* **2020**, *34*, 742–768. [CrossRef]

19. Covid-19: Race to eucalyptus in Maputo–Watch. *Club of Mozambique*, 13 April 2020; p. 1.

20. Vecchio, M.G.; Loganes, C.; Minto, C. Beneficial and Healthy Properties of Eucalyptus Plants: A Great Potential Use. *Open Agric. J.* **2016**, *10*, 52–57. [CrossRef]

21. Salehi, B.; Sharifi-Rad, J.; Quispe, C.; Llaique, H.; Villalobos, M.; Smeriglio, A.; Trombetta, D.; Ezzat, S.M.; Salem, M.A.; Zayed, A.; et al. Insights into Eucalyptus genus chemical constituents, biological activities and health-promoting effects. *Trends Food Sci. Technol.* **2019**, *91*, 609–624. [CrossRef]

22. The Jakarta Post. Available online: https://www.thejakartapost.com/news/2020/05/09/agriculture-ministry-claims-to-have-developed-eucalyptus-based-covid-19-treatment.html (accessed on 21 July 2020).

23. Tempo Misleading: COVID-19 Can Be Cured with Eucalyptus Oil. Available online: https://www.poynter.org/?ifcn_misinformation=covid-19-can-be-cured-with-eucalyptus-oil (accessed on 17 July 2020).

24. Adeniyi, B.A.; Ayepola, O.O.; Adu, F.D. The antiviral activity of leaves of Eucalyptus camaldulensis (Dehn) and Eucalyptus torelliana (R. Muell). *Pak. J. Pharm. Sci.* **2015**, *28*, 1773–1776.

25. Usachev, E.V.; Pyankov, O.V.; Usacheva, O.V.; Agranovski, I.E. Antiviral activity of tea tree and eucalyptus oil aerosol and vapour. *J. Aerosol Sci.* **2013**, *59*, 22–30. [CrossRef]

26. Kim, S.; Chen, J.; Cheng, T.; Gindulyte, A.; He, J.; He, S.; Li, Q.; Shoemaker, B.A.; Thiessen, P.A.; Yu, B.; et al. PubChem 2019 update: Improved access to chemical data. *Nucleic Acids Res.* **2019**, *47*, D1102–D1109. [CrossRef] [PubMed]

27. Hanwell, M.D.; Curtis, D.E.; Lonie, D.C.; Vandermeersch, T.; Zurek, E.; Hutchison, G.R. Avogadro: An advanced semantic chemical editor, visualization, and analysis platform. *J. Cheminform.* **2012**, *4*, 17. [CrossRef] [PubMed]

28. Jin, Z.; Du, X.; Xu, Y.; Deng, Y.; Liu, M.; Zhao, Y.; Zhang, B.; Li, X.; Zhang, L.; Peng, C.; et al. Structure of Mpro from SARS-CoV-2 and discovery of its inhibitors. *Nature* **2020**, *582*, 289–293. [CrossRef]

29. Tahir ul Qamar, M.; Alqahtani, S.M.; Alamri, M.A.; Chen, L.-L. Structural basis of SARS-CoV-2 3CLpro and anti-COVID-19 drug discovery from medicinal plants. *J. Pharm. Anal.* **2020**, *10*, 313–319. [CrossRef] [PubMed]

30. Morris, G.M.; Huey, R.; Lindstrom, W.; Sanner, M.F.; Belew, R.K.; Goodsell, D.S.; Olson, A.J. AutoDock4 and AutoDockTools4: Automated docking with selective receptor flexibility. *J. Comput. Chem.* **2009**, *30*, 2785–2791. [CrossRef]

31. Morris, G.M.; Goodsell, D.S.; Halliday, R.S.; Huey, R.; Hart, W.E.; Belew, R.K.; Olson, A.J. Automated docking using a Lamarckian genetic algorithm and an empirical binding free energy function. *J. Comput. Chem.* **1998**, *19*, 1639–1662. [CrossRef]

32. Du, X.; Li, Y.; Xia, Y.-L.; Ai, S.-M.; Liang, J.; Sang, P.; Ji, X.-L.; Liu, S.-Q. Insights into Protein–Ligand Interactions: Mechanisms, Models, and Methods. *Int. J. Mol. Sci.* **2016**, *17*, 144. [CrossRef]

33. Laskowski, R.A.; Swindells, M.B. LigPlot+: Multiple Ligand–Protein Interaction Diagrams for Drug Discovery. *J. Chem. Inf. Model.* **2011**, *51*, 2778–2786. [CrossRef]

34. Hess, B.; Bekker, H.; Berendsen, H.J.C.; Fraaije, J.G.E.M. LINCS: A linear constraint solver for molecular simulations. *J. Comput. Chem.* **1997**, *18*, 1463–1472. [CrossRef]

35. Miyamoto, S.; Kollman, P.A. Settle: An analytical version of the SHAKE and RATTLE algorithm for rigid water models. *J. Comput. Chem.* **1992**, *13*, 952–962. [CrossRef]

36. Schmid, N.; Eichenberger, A.P.; Choutko, A.; Riniker, S.; Winger, M.; Mark, A.E.; van Gunsteren, W.F. Definition and testing of the GROMOS force-field versions 54A7 and 54B7. *Eur. Biophys. J.* **2011**, *40*, 843–856. [CrossRef] [PubMed]

37. Muhammad, A.; Khunrae, P.; Sutthibutpong, T. Effects of oligolignol sizes and binding modes on a GH11 xylanase inhibition revealed by molecular modeling techniques. *J. Mol. Model.* **2020**, *26*, 124. [CrossRef] [PubMed]

38. Kumari, R.; Kumar, R.; Lynn, A. g_mmpbsa—A GROMACS Tool for High-Throughput MM-PBSA Calculations. *J. Chem. Inf. Model.* **2014**, *54*, 1951–1962. [CrossRef] [PubMed]

39. Kumar, A.; Choudhir, G.; Shukla, S.K.; Sharma, M.; Tyagi, P.; Bhushan, A.; Rathore, M. Identification of phytochemical inhibitors against main protease of COVID-19 using molecular modeling approaches. *J. Biomol. Struct. Dyn.* **2020**, 1–11. [CrossRef]

40. Meng, X.-Y.; Zhang, H.-X.; Mezei, M.; Cui, M. Molecular docking: A powerful approach for structure-based drug discovery. *Curr. Comput. Aided Drug Des.* **2011**, *7*, 146–157. [CrossRef]

41. Sethi, A.; Joshi, K.; Sasikala, K.; Alvala, M. Molecular docking in modern drug discovery: Principles and recent applications. In *Drug Discovery and Development-New Advances*; IntechOpen: Rijeka, Croatia, 2019.

42. Das, P.; Majumder, R.; Mandal, M.; Basak, P. In-Silico approach for identification of effective and stable inhibitors for COVID-19 main protease (Mpro) from flavonoid based phytochemical constituents of Calendula officinalis. *J. Biomol. Struct. Dyn.* **2020**, 1–16. [CrossRef]

43. Mpiana, P.T.; Ngbolua, K.-T.-N.; Tshibangu, D.S.T.; Kilembe, J.T.; Gbolo, B.Z.; Mwanangombo, D.T.; Inkoto, C.L.; Lengbiye, E.M.; Mbadiko, C.M.; Matondo, A.; et al. Identification of potential inhibitors of SARS-CoV-2 main protease from Aloe vera compounds: A molecular docking study. *Chem. Phys. Lett.* **2020**, *754*, 137751. [CrossRef]

44. Gurung, A.B.; Ali, M.A.; Lee, J.; Farah, M.A.; Al-Anazi, K.M. Unravelling lead antiviral phytochemicals for the inhibition of SARS-CoV-2 Mpro enzyme through in silico approach. *Life Sci.* **2020**, *255*, 117831. [CrossRef]

45. Gajula, M.N.V.P.P.; Kumar, A.; Ijaq, J. Protocol for Molecular Dynamics Simulations of Proteins. *Bio-Protocol* **2016**, *6*, e2051. [CrossRef]

46. Ning, X.; Zhang, Y.; Yuan, T.; Li, Q.; Tian, J.; Guan, W.; Liu, B.; Zhang, W.; Xu, X.; Zhang, Y. Enhanced Thermostability of Glucose Oxidase through Computer-Aided Molecular Design. *Int. J. Mol. Sci.* **2018**, *19*, 425. [CrossRef]

47. English, A.C.; Groom, C.R.; Hubbard, R.E. Experimental and computational mapping of the binding surface of a crystalline protein. *Protein Eng. Des. Sel.* **2001**, *14*, 47–59. [CrossRef] [PubMed]

48. Sang, P.; Tian, S.-H.; Meng, Z.-H.; Yang, L.-Q. Anti-HIV drug repurposing against SARS-CoV-2. *RSC Adv.* **2020**, *10*, 15775–15783. [CrossRef]

49. Al-Khafaji, K.; Al-Duhaidahawi, D.; Taskin Tok, T. Using integrated computational approaches to identify safe and rapid treatment for SARS-CoV-2. *J. Biomol. Struct. Dyn.* **2020**, 1–9. [CrossRef] [PubMed]

50. Bhardwaj, V.K.; Singh, R.; Sharma, J.; Rajendran, V.; Purohit, R.; Kumar, S. Identification of bioactive molecules from tea plant as SARS-CoV-2 main protease inhibitors. *J. Biomol. Struct. Dyn.* **2020**, 1–10. [CrossRef] [PubMed]

51. Dash, J.J.; Purohit, P.; Muya, J.T.; Meher, B.R. Drug Repurposing of Allophenylnorstatine Containing HIV-Protease Inhibitors Against SARS-CoV-2 Mpro: Insights from Molecular Dynamics Simulations and Binding Free Energy Estimations. *ChemRxiv* **2020**. [CrossRef]

52. Joshi, T.; Sharma, P.; Joshi, T.; Pundir, H.; Mathpal, S.; Chandra, S. Structure-based screening of novel lichen compounds against SARS Coronavirus main protease (Mpro) as potentials inhibitors of COVID-19. *Mol. Divers.* **2020**, 1–13. [CrossRef]